Onset of the excluded-volume effect for the statistics of stiff chains

Jangnyeol Moon and Hisao Nakanishi
Department of Physics, Purdue University, West Lafayette, Indiana 47907
(Received 17 May 1991)

We investigate the conformation of very stiff chains with increasing molecular weight focusing on the onset of the excluded-volume effect. A Flory argument is given for the case in which the shape of monomers has a disklike anisotropy, which causes the excluded-volume effect to set in for shorter chains. A scaling argument determines the exponent associated with the anisotropy in terms of the main exponent that controls the onset of the excluded-volume effect. We suggest a way of viewing the stiff chain as a train of mutually repelling blobs and reanalyze some data in the experiment of Murakami, Norisuye, and Fujita [Macromolecules **13**, 345 (1980)]. An extensive Monte Carlo simulation of the persistent self-avoiding walk (PSAW) has been performed on cubic and diamond lattices. We find an extremely gradual crossover of the Flory exponent from the Gaussian value ($\nu_F = \frac{1}{2}$) to the full self-avoiding one ($\nu_F \approx \frac{3}{5}$) as the chain becomes longer. Finally, we present an approximate analytic calculation of the attrition rate of an equivalent flight model for the PSAW.

PACS number(s): 05.50.+q, 61.41.+e, 64.60.Fr

I. INTRODUCTION

A main interest in studying the conformation of stiff linear polymers in dilute solutions has been in the effect of stiffness on the scaling of the size of the chain. Stiff linear polymers are often called wormlike, semiflexible, or rodlike [1–6]. The stiffness in equilibrium is usually described by rotational isomeric states [7–9], i.e., a monomer-monomer link in a certain local orientation is favored depending on the energy configuration of the component atoms in the environment. Thus the thermal mean conformation of the polymer tends to persist in one direction. The mean length of this straight segment is usually called a *persistence length*, which is a measure of the stiffness.

One may easily predict that for strong stiffness and small molecular weight, the size of a single polymer (e.g., end-to-end distance or the radius of gyration) will scale like a straight rod. However, for large molecular weight with fixed stiffness, the chain could be described as a random walk with a variable step size whose mean corresponds to the persistence length, if the excluded-volume effect is ignored. These descriptions also apply to other properties of the polymer, such as the intrinsic viscosity and sedimentation coefficients which correspond to different moments of the monomer-monomer distance distribution. Indeed, some analytic expressions of end-to-end distance of a stiff chain in terms of the contour length are well known for certain non-excluded-volume random-walk models [8, 10–12], and they tend to accurately describe the crossover between rodlike regime to flexible (random-walk-like) regime.

In a real polymer, however, two monomers cannot occupy the same space at the same time, and the conformation of the polymer will be affected by this excluded-volume effect [7–9] in the flexible regime and beyond.

General features of the behavior of the linear stiff chain in $d = 3$ can be sketched as in Fig. 1, where the end-to-end distance (or the radius of gyration) R is plotted against the degree of polymerization N in the double logarithmic scale. There are three distinct regimes [13, 14] if the chain is sufficiently stiff, namely, rodlike ($R^2 \sim N^2$), Gaussian ($R^2 \sim N$), and excluded-volume ($R^2 \sim N^{2\nu}$) regimes. The crossovers between these successive regimes are called rod-to-flexible and Gaussian–to–excluded-volume, respectively. The Gaussian regime

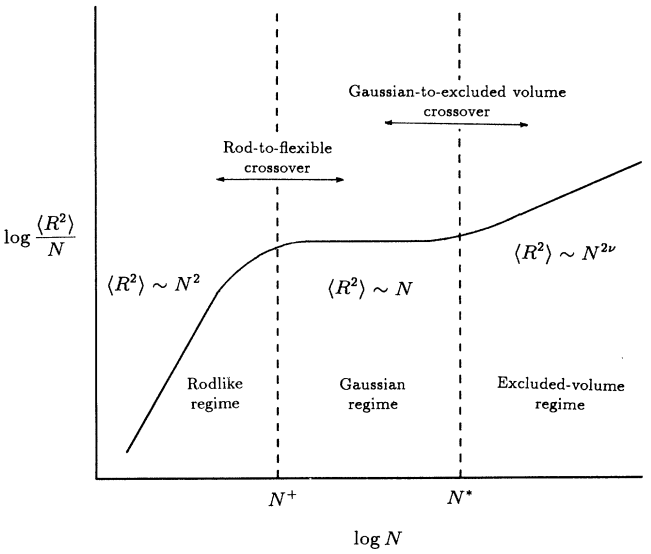

FIG. 1. General behavior of the end-to-end distance R of very stiff linear polymers as a function of the degree of polymerization N in three dimensions is plotted in double logarithmic scale. Three distinct regimes and two crossovers between them are termed as in the figure. N^+ and N^* are typical values of N where corresponding crossovers occur. In two dimensions, the Gaussian regime is known to be nonexistent.

is not strictly the same as the non-excluded-volume case, rather, it corresponds to an asymptotic behavior of a very stiff and very long chain. Moreover, it is well known that the Gaussian regime does not exist in $d = 2$.

In this paper, we will study the onset of the excluded-volume effect for the statistics of stiff chains mainly in the framework of the persistent self-avoiding walk model (PSAW) first proposed by Halley, Nakanishi, and Sundararajan [15]. In the PSAW model, a walk is realized on a discrete lattice by making individual steps which, with no immediate backtracking, choose a different direction than the previous one with a probability p (*gauche* step) or go straight in the same direction as before with a probability $1 - p$ (*trans* step). If this walk does not intersect itself then it is taken as a valid member of the ensemble, and otherwise it is discarded.

The original scaling ansatz [15] for the end-to-end distance of PSAW was written as

$$\langle R^2 \rangle = N^{2\nu} p^{(2\nu-2)\Delta} F(Np^{\Delta}), \tag{1}$$

where N is the number of steps, ν is the Flory exponent, and Δ is a crossover exponent. This is an asymptotic expression in the limit of

$$N \to \infty, \quad p \to 0 \quad \text{with } Np = \text{const.} \tag{2}$$

Various approaches, such as series enumeration [16], renormalization [13], and Monte Carlo simulations [12, 15], have been applied to find $F(x)$. They all agree that $\Delta = 1$ exactly and the behavior of $F(x)$ for $x \ll 1$ is such that $\langle R^2 \rangle \sim N^2$ in all dimensions. However, its behavior for $x \gg 1$ strongly depends on the dimensionality [12]. In two dimensions, $F(x)$ rapidly saturates to a constant. For three dimensions, it is rather convenient to rewrite Eq. (1) as

$$\langle R^2 \rangle = \frac{N}{p} \tilde{F}(Np), \tag{3}$$

where $\tilde{F}(x) \sim x$ for $x \ll 1$ and $\tilde{F}(x) \sim$ const for $x \gg 1$ in the limit (2).

It should be noted that $\tilde{F}(x)$ is different from the Gaussian persistent-random-walk (or PRW) scaling function,

$$F_0(x) = 2(e^{-x} + x - 1)/x, \tag{4}$$

in that, even though their small-x behaviors are the same, $F_0(x)$ approaches 2 for large x while $\tilde{F}(x)$ approaches a (lattice-dependent) constant greater than 2 in the limit (2). This discrepancy is obviously due to the excluded-volume effect which is not yet significant enough to give the Flory exponent greater than the Gaussian value $\nu_0 = \frac{1}{2}$. Thus, even though the region $x \gg 1$ in the limit (2) is often called the Gaussian regime, the scaling function is not identical to that of PRW.

For any finite and fixed p, the excluded-volume effect will eventually dominate as N goes to infinity and a second crossover (Gaussian–to–excluded-volume crossover) is expected [13, 17] to occur. Such a crossover may be controlled by a variable $N^* \equiv Np^y$ for some $y > 1$ such that the full SAW value of the Flory exponent is recovered for $N \gg N^*$. Correspondingly, we expect that there exists another scaling function in the limit

$$N \to \infty, \quad p \to 0 \quad \text{with } Np^y = \text{const} \quad (y > 1). \tag{5}$$

It has been suggested [14] that this second limit could be incorporated together with the first limit in a single scaling function of the form

$$\langle R^2 \rangle = \frac{N}{p} a^2 h(Np, Np^y), \tag{6}$$

where a is the size of a monomer or the lattice constant in the PSAW model and $N^* \sim p^{-y}$ can be considered as a scale for the number of monomers where the second crossover begins to occur.

Since, in the limit (2) we have $Np^y \to 0$, the scaling form (3) is clearly consistent with Eq. (6). In the limit (5), we have $Np \to \infty$, and again Eq. (6) can be used if we assume no singularity for h in this limit. In the latter limit, Eq. (6) reduces to an expression for the excluded-volume regime:

$$\langle R^2 \rangle = \frac{N}{p} a^2 \overline{h}(Np^y). \tag{7}$$

Furthermore, assuming that $\overline{h}(x)$ has a power-law behavior for large x and requiring that $\langle R^2 \rangle \propto N^{2\nu}$, we are led to a scaling relation [14]

$$\langle R^2 \rangle \sim N^{2\nu} p^{-\alpha} a^2, \quad Np^y \to \infty, \tag{8}$$

where $\alpha = 1 - (2\nu - 1)y$ ($\alpha = \frac{2}{5}$ in $d = 3$ by the Flory approximation).

Previously, simulation [12], series-expansion [18], and renormalization [13] calculations indicated that there exist significant differences between two and three dimensions in the way the crossovers occur. While the excluded-volume regime immediately follows the stiff regime in $d = 2$, there is a Gaussian regime in between the two crossovers in $d = 3$. This point is supported by the Flory approximation [17] in that both limits (2) and (5) become identical in $d = 2$ while they do not in higher dimensions.

Indeed, a previous numerical work [14] observed the onset of the Gaussian–to–excluded-volume crossover in the three-dimensional PSAW model. In that calculation, a crude numerical estimate of exponent y [cf. the limit (5)] was given, which was significantly smaller than the Flory value ($y = 3$ in $d = 3$). On the other hand, an experiment on a real stiff polymer has been reported [19], where the full excluded-volume effect is observed for much shorter chains than their PSAW counterparts. A more extensive calculation of the exponent y as well as a discussion of this latter point will be presented later in this paper.

We will also study the question of universality [20] for the stiff chains. The lattice dependence of the scaling function serves as a good criterion to determine whether there exists universality for the PSAW model. We will use the terminology where the *strong* universality means not only the exponent but also the functional form of the scaling function should be independent of the type of lattice (up to *metrical* factors), while the *weak* univer-

sality does not require the latter. It is well known that strong universality of the end-to-end distance and the radius of gyration holds for the stiff chains which are not self-avoiding. This means that within the PRW model, Eq.(4) holds for many different lattices with only very mild modifications according to the definition of *gauche* and *trans* steps (e.g., see Schroll, Walker, and Thorpe [10] for the diamond lattice).

While there are not many simulation studies of strong universality for PRW or PSAW models reported, series enumeration study [16] for the PSAW on square and triangular lattice finds it impossible to obtain strong universality. Apart from the PSAW model, the exact solutions [6, 21] of some directed-walk models also indicate that there is no strong universality between square and triangular lattices and the dimension dependence of hypercubic lattices vanishes only in the limit $d \to \infty$.

Thus, the organization of this paper is as follows: In Sec. II, we discuss the theoretical results. In particular, we present the extension of the Flory argument for the case in which the monomer has a disklike anisotropy in its shape. Also, a way of viewing the stiff chains as a train of mutually repelling blobs is suggested. Section III is the major part of this paper: Results and analyses of our Monte Carlo simulation for the three-dimensional PSAW model are presented including the end-to-end distances, exponent ν and γ, lattice dependence, and scaling function $\tilde{F}(Np)$ [Eq.(3)]. We also present an approximate analytic calculation of the attrition rate of a certain self-avoiding flight model (which is asymptotically equivalent to the PSAW model with a simple rescaling of the contour length). This calculation allows us to determine a lower limit for the exponent y in Eq. (5). In Sec. IV, the experimental data from Murakami, Norisuye, and Fujita [19] are reanalyzed and some possible interpretations for the observed Gaussian–to–excluded-volume crossover are suggested. Section V is devoted to summary and discussion.

II. THEORETICAL RESULTS

We consider a linear polymer model whose monomers have a disklike anisotropy and attach face to face so that a segment forms a straight cylindrical rod. Let a be the thickness and D the diameter of a monomer. Then the ratic $b \equiv D/a$ can be used as a measure of the monomer anisotropy and the average length of the segment (persistent length) $l_p \equiv a/p$ may effectively represent the stiffness of the polymer in terms of the *gauche* probability as in the PSAW model. This is of course a very simplified picture compared with real polymers. However, we assume that the persistent length is much larger than the diameter of the monomer so that the details around joints between the two adjacent straight segments may be considered unimportant.

We apply the Flory argument for this case to derive a scaling expression of the end-to-end distance as a function of the number of monomers N and above parameters p, b, and a. First, we write down the free energy of a single polymer as a sum of interaction and elastic (entropic) parts:

$$F = F_{\rm int} + F_{\rm el}. \tag{9}$$

The interaction part is proportional to Odijk and Houwaart's excluded volume [22] (per persistence length), which can be generalized in d dimensions as

$$\Omega \propto l_p^2 D^{d-2} = \frac{a^2}{p^2} D^{d-2}. \tag{10}$$

Thus in the Flory approximation,

$$F_{\rm int}/k_B T \sim \frac{(Np)^2 \Omega}{R^d} = \frac{N^2 a^2 D^{d-2}}{R^d}, \tag{11}$$

and

$$F_{\rm el}/k_B T \sim \frac{(R/l_p)^2}{Np} = \frac{R^2 p}{N a^2}. \tag{12}$$

Substituting the above expressions into Eq. (9) and minimizing F with respect to R, we get the end-to-end distance

$$R \sim N^{3/(d+2)} p^{-1/(d+2)} b^{(d-2)/(d+2)} a. \tag{13}$$

It should be noted that this relation is valid, if at all, asymptotically for large N for which it is required that $F_{\rm int}(N) \gg 1$. This allows us to define N^* such that $F_{\rm int}(N^*) \sim 1$ and to obtain, from Eqs. (11) and (13),

$$N^* p \sim (bp)^{-2(d-2)/(4-d)}. \tag{14}$$

Thus the Flory expression (13) is intended only for $N \gg N^*$.

The form (14) suggests a more general form beyond the Flory approximation:

$$N^* p \sim (bp)^{-z}, \tag{15}$$

for some yet unknown exponent z. Treating the N^* as the crossover size discussed in Eqs. (6) and (7), we then identify

$$z = y - 1. \tag{16}$$

Again a simple scaling argument that was used in deriving Eq. (8), with Np^y replaced by N/N^*, leads to another scaling relation incorporating the monomer anisotropy:

$$R^2 \sim N^{2\nu} p^{-\alpha} b^{\beta} a^2, \tag{17}$$

where α is the same as in Eq. (8) and $\beta = (y-1)(2\nu-1)$. It should be noted that Eq. (13) is recovered from this expression if the Flory values of ν and y are used in it.

As it turns out, Eqs. (17) and (8) are nothing more than a result of a simple rescaling of variables in each other. Suppose that l_p is sufficiently larger than D so that the polymer with anisotropic monomers can be viewed as that with *isotropic* monomers of size D with the number of monomers reduced by a factor of b, that is, b anisotropic monomers stick together to make one isotropic *block* of size D. Then the variables (p, N, a, b) in the original problem with anisotropic monomers can be rescaled to obtain those in a new problem with isotropic blocks $(p', N', a', 1)$ as follows:

$$\begin{aligned} p &\to p' = bp, \\ N &\to N' = N/b, \\ a &\to a' = D = ba, \\ b &\to 1. \end{aligned} \tag{18}$$

Using this rescaling and knowing that the end-to-end distance is unchanged under the rescaling, we can deduce Eq. (16) from Eq. (7) and Eq. (17) from Eq. (8) for instance.

We now develop a way of viewing the stiff chain problem in a *blob* picture. Let us consider a train of mutually repelling blobs which perform an ordinary self-avoiding walk. Moreover, suppose the blobs themselves are made up of a stiff self-avoiding chain in the Gaussian regime. We suppose that each blob contains N^* monomers so that the number of persistence length segments within a blob is

$$g_s = N^* p \sim p^{1-y} \gg 1, \tag{19}$$

for small p. We always assume that there are a large number of persistent length segments in the whole chain (i.e., $Np \gg 1$), but the number of *blobs* may not be large.

If the number of blobs is large (i.e., $N/N^* \gg 1$), then the size of the chain can be written as

$$\langle R^2 \rangle \sim N_B^{2\nu} \xi^2, \tag{20}$$

where N_B is the number of blobs in a polymer with N monomers and ξ is the average size of a blob. Given that

$$N_B = N/N^* \sim N p^y, \tag{21}$$

and using the non-excluded-volume random-walk relation

$$\xi \sim g_s^{\frac{1}{2}} l_p \sim p^{-(y+1)/2} a, \tag{22}$$

where Eq. (19) is used for g_s, one immediately sees that Eq. (20) reproduces Eq. (8). Moreover, it can be shown that Eq. (20) leads to Eq. (17) applying the rescaling rule (19) to N_B and ξ for the case of the anisotropic monomer.

If, on the other hand, the number of blobs is small (i.e., $N/N^* \sim 1$ or less), then the size of the chain is

$$\langle R^2 \rangle \sim (Np) l_p^2 \sim \frac{N}{p} a^2, \tag{23}$$

which is just Eq. (3). Thus this blob picture is consistent with the whole range of the crossover.

Now, the number of monomers per blob for the PSAW model, $N^* \sim p^{-y}$, appears to be smaller than the Flory approximation prediction since the lattice calculations show (see later) that the actual value of y is less than the Flory prediction of 3. This kind of discrepancy may be due to the nature of the segment size distribution of the PSAW model. Unlike in the Flory argument which assumes uniform segment size, the actual distribution is exponential, generating a large majority of segments shorter than the mean. Thus it is not unreasonable that a smaller number of monomers than the Flory argument suggests are sufficient to yield the flexible, excluded-volume behavior.

Even though the blob picture produces consistent scaling forms for the end-to-end distance [Eqs. (8) and (17)] in the excluded-volume limit (5), it is undeniable that the blob is not a physically well-defined object having in particular a clear-cut geometrical boundary. Thus this idea is only intended to illustrate the behavior of the stiff chain at different length scales and not meant to be a faithful physical picture which could be experimentally verified. If it were to have some direct significance at all, it would at best be approximate in the sense that these blobs must significantly overlap, thus depressing the prefactor in Eq. (20).

III. MONTE CARLO SIMULATION

We generate PSAW's on the simple-cubic (sc), the body-centered-cubic (bcc), the face-centered-cubic (fcc), and the diamond lattice for various *gauche* probabilities (p). A major difficulty in realizing a large number of long self-avoiding walks, as far as the computing time is concerned, is that the loop checking should be performed each time a new step is generated and if the intersection occurs the whole walk stops growing, so that only a small fraction of walkers starting at the origin will survive the self-avoiding constraint to make a long walk. This situation has been greatly improved by use of the enrichment technique [23] for the attrition rate and the hash-coding method for the loop-checking routine. (See Appendix B.)

For the case of PSAW, however, one encounters another difficulty: Even if the attrition is greatly reduced as p becomes smaller, N should be very large to get data for a finite value of Np, which renders the loop-checking for $Np \gg 1$ highly time-consuming even with the enrichment technique and the hash-coding method being used. To further improve this situation for very stiff chains, we consider a random-flight model whose *segment* size distribution is the same as that of the persistence length of PSAW:

$$P(l) = p(1-p)^{l-1}, \quad l = 1, 2, 3, \ldots . \tag{24}$$

Thus in this flight model, a straight segment consisting of l individual steps can be generated by a single random number according to the above distribution always making a turn in a randomly chosen direction different from that of the previous segment. (Backtracking is precluded in any case.) Removing all self-intersecting flights from this ensemble will produce the ensemble for the corresponding self-avoiding-flight model. The loop-checking is also done by segment as in Ref. [24] partially using the hash-coding method.

We match the uniform random number r between 0 and 1 to the segment size l as follows: Since r is continuous down to the order of the inverse of the largest integer that a computer in use can create, we consider a probability density function $P'(l')$ defined for a real number

$l' \geq 0.5$ onto which r is to be mapped. For each l', its nearest integer is chosen as the segment size. Therefore it is required that

$$\int_{l-0.5}^{l+0.5} P'(l')\,dl' = P(l), \quad l = 1,2,3,\ldots \tag{25}$$

where $P(l)$ is as defined in Eq. (24) and thus ensures the normalization of $P'(l')$. The relation between r and l' is found by

$$P'(l')\,dl' = dr \tag{26}$$

with an appropriate boundary condition. One can easily determine $P'(l')$ starting from an ansatz having the same form of Eq. (24):

$$P'(l') = \left(\ln\frac{1}{1-p}\right)(1-p)^{l'-0.5}, \tag{27}$$

which in turn gives l' in terms of r,

$$l' = \frac{1}{2} + \frac{\ln(1-r)}{\ln(1-p)}. \tag{28}$$

The data for PSAW are obtained from this flight simulation by keeping track of the contour length of the flight every time a new segment is generated. Details of the parameters in the simulation and the computing times are given in Appendix B. The data by segments for this type of flight might also be of interest by itself and more importantly in relation to the behavior of the PSAW as a function of mean number of persistent segments, i.e., Np. We will discuss more on this point later in this section.

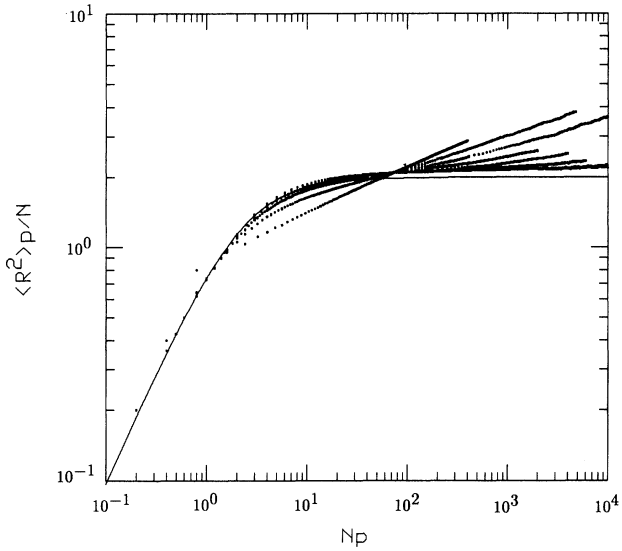

FIG. 2. Mean-square end-to-end distance of the PSAW on the simple cubic lattice against the mean number of segment Np is shown for $p = 0.8, 0.4, 0.2, 0.1, 0.05, 0.02, 0.01$ in the order of higher slope beyond the Gaussian regime ($Np \gg 1$). $p = 0.8$ corresponds to the normal SAW for which $\nu_F \approx 0.59$. Solid line is the exact result of the PRW [Eq. (4)] in the limit (2). The excluded-volume effect sets in, if very slowly, as the chain becomes longer.

One of the main results of our simulation pertains to the end-to-end distance and the related exponent ν. Figure 2 shows the result for the end-to-end distance of the PSAW on the simple cubic lattice against the mean number of persistent segments in the log-log plot. The solid line is the exact PRW result in the limit (2), which is Eq. (4). The *gauche* probabilities used are $p = 0.8, 0.4, 0.2, 0.1, 0.05, 0.02, 0.01$ where $p = 0.8$ corresponds to the ordinary SAW. Data for $p \leq 0.1$ were obtained mainly from the flight simulation. Maximum Np for our data is 10^4 so that the maximum step is one million for $p = 0.01$ and we generated more than 80 000 realizations of it. In this figure, one can clearly see the crossovers between three distinct regimes as the chain gets longer and stiffer but the final excluded-volume regime sets in for extremely long chains as the local slope increases very slowly toward the full SAW value ($\nu \approx 0.59$).

To study this feature in terms of the exponent itself, it is convenient to examine the effective exponent ν_N defined as follows:

$$\nu_N = \frac{N\langle R_N^2\rangle}{2\int_0^N \langle R_N^2\rangle dN} - \frac{1}{2}. \tag{29}$$

This definition reflects the main exponent and the correction-to-scaling in its asymptotic form,

$$\nu_N = \nu + C_\Delta N^{-\Delta_1} + C_1 N^{-1} + \cdots, \tag{30}$$

if there is a power-law correction with an exponent $\Delta_1 < 1$.

Figure 3 shows the effective exponent ν_N defined by Eq. (29) for $p = 0.8, 0.4, 0.2, 0.1$ against the inverse of

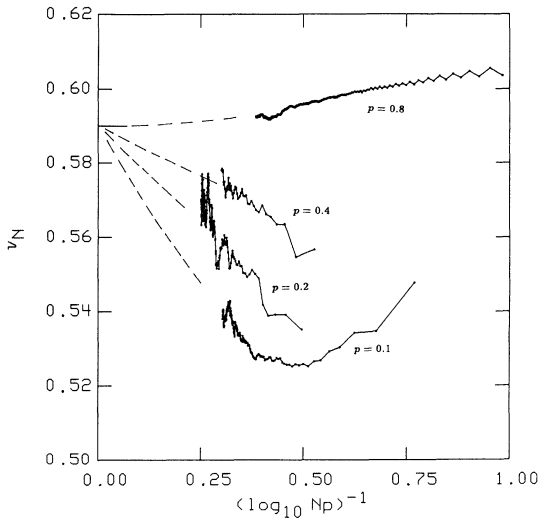

FIG. 3. The effective Flory exponent ν_N defined by Eq. (29) of the PSAW on the simple cubic lattice is plotted against the inverse log of Np. Dashed lines are drawn for a visual aid showing the general tendency of the asymptotic behavior of ν_N which approaches the ordinary SAW value of ν (≈ 0.59) as $N \to \infty$ for fixed p.

the logarithm of Np. The integration in the definition of ν_N is done using Simpson's rule and we retain the result of the computation for chains of up to a reasonable length so that the wildly fluctuating behavior for the very long chains (which is essentially statistical error) should not obscure the general feature. One can readily see this general feature that ν_N tends to approach the full SAW value ($\nu \approx 0.59$) as suggested by the dashed lines in the figure even if their intermediate values are smaller for all $p < 0.8$.

For lattices other than simple cubic, we present the end-to-end distance data for $p = 0.1$ and 0.01 to check for the universality. The ratio of the mean-square end-to-end distance of the PSAW ($\langle R^2 \rangle$) to that of the PRW ($\langle R_0^2 \rangle$) is shown in Fig. 4 against the logarithm of Np, where

$$\langle R_0^2 \rangle p/N = 2 - p - \frac{2(1-p)}{Np}\left[1 - (1-p)^N\right] \qquad (31)$$

for sc, bcc, and fcc lattices but we used Schroll, Walker, and Thorpe's result [Eq. (20) of Ref. [10]] for $\langle R_0^2 \rangle$ on the diamond lattice. Note that $\langle R^2 \rangle$ deviates from $\langle R_0^2 \rangle$ in a similar manner for all lattices. Particularly, the amplitudes of the scaling functions for different lattices appear to be different only by some metric factors from one another for $Np \gtrsim 10$. Thus it seems that even though strong universality does not hold over the rodlike to Gaussian regimes it might hold over the Gaussian–to–excluded-volume regimes. If this were the case, the scaling functions of PSAW in the limit (5) would be of the same form (apart from some metric factors).

Another interesting point in Fig. 4 is that the results for sc and fcc lattices are particularly similar to each other. Whether this is a mere accident or something that can be explained by more direct geometrical considerations is not clear at present.

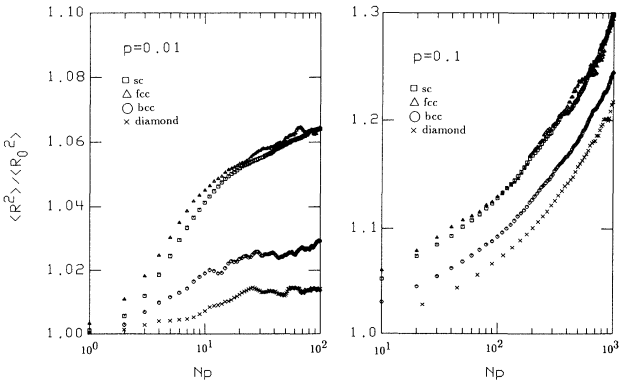

FIG. 4. The ratio of the mean-square end-to-end distance of the PSAW to that of the PRW on the cubic and the diamond lattices against Np for $p = 0.1$ and 0.01. The latter case shows the rod-to-flexible crossover and the former the Gaussian–to–excluded-volume crossover.

We now examine the excluded-volume effect more quantitatively using numerical methods. As pointed out in the Introduction, the excluded-volume effect in the limit (2) is totally suppressed as far as the exponent ν is concerned even if $\langle R^2 \rangle p/N$ is always larger than $F_0(Np)$ [Eq. (4)] and quickly approaches a constant greater than 2 as $Np \to \infty$. From mere observation that the amplitude of $\langle R^2 \rangle p/N$ [$\tilde{F}(Np)$ in Eq. (3)] saturates toward a constant in a way similar to the PRW and requiring one additional condition that $\tilde{F}(Np) \to 1$ as $Np \to 0$, we suggest an approximate form of $\tilde{F}(Np)$ as follows:

$$\tilde{F}(x) \approx \frac{1}{\kappa} F_0(\kappa x), \qquad (32)$$

where $F_0(x)$ is the scaling function for the PRW [Eq. (4)]. This corresponds to replacing the left-hand side of Eq. (3) with the Gaussian result with some effective *gauche* probability $p' = \kappa p < p$, which is essentially a mean-field-like approximation where the swelling of a chain due to the excluded-volume effect is expressed in terms of an increase of stiffness of the corresponding Gaussian chain imposing correct limiting behaviors.

We attempt to fit for κ using our data with $p = 10^{-2}$ and Np up to 100. The result is $\kappa_{sc} \approx 0.948, \kappa_{fcc} \approx 0.942, \kappa_{bcc} \approx 0.975, \kappa_{dia} \approx 0.989$. (The right variable of the scaling function for the diamond lattice is $Np/2$. See Schroll, Walker, and Thorpe [10].) With the self-avoiding *flight* algorithm on the simple-cubic lattice, we could further probe into the limit (2) like $p = 10^{-4}, 10^{-6}$ with Np up to 10^3 but only obtain very similar values.

Finding out the scaling function in the limit (5) is an even more difficult task. Exponent y should be determined first and then the functional form of the end-to-end distance in terms of Np^y. In the previous work, an attempt to numerically determine y was made by examining the best data collapse between absolute values of $\langle R^2 \rangle p/N$ for different p's in the region $Np \gg 1$, which gave rise to $y \approx 2.3$. In this work, the same method using a much larger set of data appears to favor a larger value of y. Figure 5(a) clearly indicates a reasonable degree of data collapse for $Np^{2.5} > 1$ based on currently available data. Note that the larger p is, the steeper is the slope of the curve over the Gaussian–to–excluded-volume crossover which suggests an important requirement for the data collapse that two curves with different values of p should not cross. The magnified view of these curves in the inset of Fig. 5(a) shows that this requirement is well achieved except for the $p = 0.01$ curve. However, considering the large fluctuation of $p = 0.01$ data for $Np \gtrsim 1000$ (indicated by error bars), we believe that this single exception cannot totally invalidate our estimation for y. This value $y \approx 2.5$ is fairly close to the estimate from the experiment of Murakami, Norisuye, and Fujita [19] using Eq. (15) with the multiplicative factor of unity discussed in the following section.

However, we note that all our data were obtained for

finite values of p but the scaling function that is to be sought is meant for the limit (5). Thus we try $\langle R^2\rangle/\langle R_0^2\rangle$ as another scaling function, which systematically compensates the finiteness of p as in Eq. (31) still having the limiting behavior identical to that of $\langle R^2\rangle p/2N$ in the limit (5). This indeed produces a better data collapse as shown in Fig. 5(b), where the same logarithmic scale as in 5(a) is used for the ordinate. Moreover, another estimation for y follows from this new analysis, namely, $y \approx 2.9$, which is larger than the estimation based on data collapsing as discussed in the preceding paragraph ($y \approx 2.5$). It is unfortunate that our data so far obtained by consuming an enormous amount of computing time are still insufficient to numerically determine which estimation for y is better and it might be that another method like renormalization calculation is more desirable, though, in any case, y seems to lie between 2 and 3.

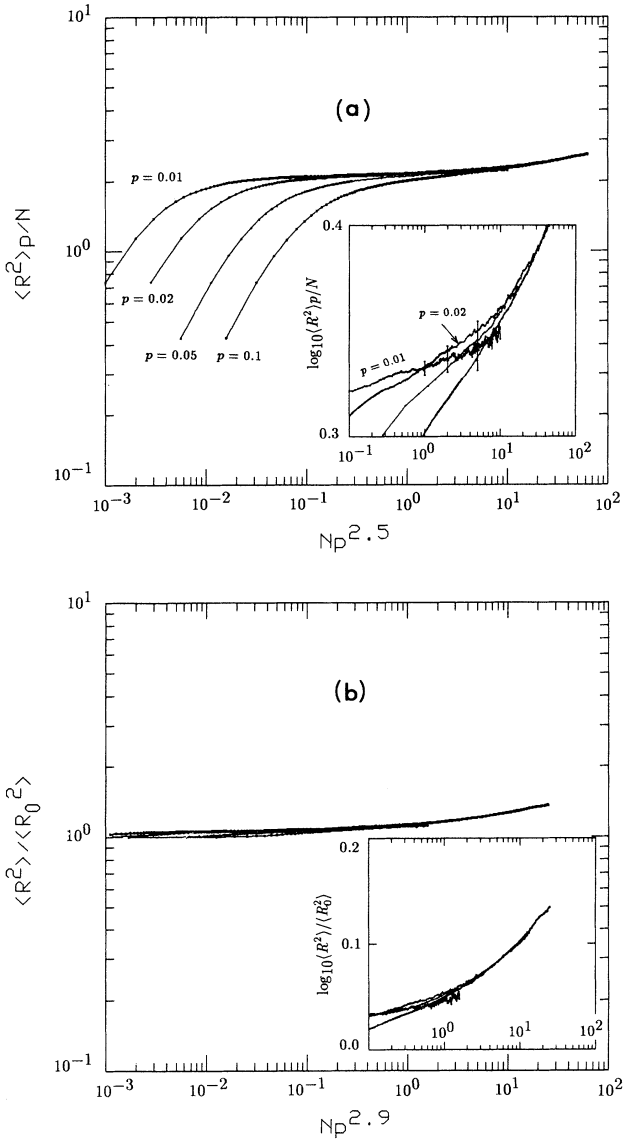

FIG. 5. The result of the PSAW on the simple cubic lattice plotted against Np^y. Exponent y is estimated numerically and takes on different values depending on how $\langle R^2\rangle$ is scaled. (a) Best data collapse over the Gaussian–to–excluded-volume crossover is achieved with $y \approx 2.5$. Maximum values of Np^y are approximately 10, 17, 48, 63 for $p = 0.01, 0.02, 0.05, 0.1$, respectively. Error bars in the inset refers to the $p = 0.01$ data. (b) $y \approx 2.9$ gives best scaling. Maximum values of Np^y are approximately 1.6, 3.6, 13.4, 25.2 for $p = 0.01, 0.02, 0.05, 0.1$, respectively.

Another important quantity that has been of great interest in the study of stiff chains is the number of configurations for walks having a given number of steps by which the exponent γ and the effective coordination number μ may be defined [Eq. (33)]. Each configuration should be appropriately weighted to account for the number of *gauche* (or *trans*) steps in it. For the PRW, one can easily verify that if the *trans* step is weighted by unity (hence each *gauche* step by $p/(1-p)(z-2)$, where z is the coordination number), then the number of N-step walks will be like e^{Np} in the limit (2) implying that $\gamma = 0$ and $\mu = e$ both being independent of lattice type. This leads us to an ansatz for the number of PSAW in the following form:

$$C_{N,p} = C(Np) \sim (Np)^{\gamma-1}\mu^{Np}. \tag{33}$$

Although this definition appears to adopt the limit (2), we will also use it for the excluded-volume regime [$N > N^*(= p^{-y})$] to examine the asymptotic behavior of γ and μ within a numerical method. For this purpose, we further define the *global* survivability as

$$S(Np) \equiv \frac{C_{\mathrm{PSAW}}}{C_{\mathrm{PRW}}} \sim (Np)^{\gamma-1}\overline{\mu}^{Np}, \tag{34}$$

where $\overline{\mu}$ is the ratio of the effective coordination number of PSAW to that of PRW, and the *local* survivability as

$$\sigma_H(Np) \equiv \frac{S(Np)}{S(Np-H)} = \left(\frac{Np}{Np-H}\right)^{\gamma-1}\overline{\mu}^{H}, \tag{35}$$

where $H \geq 1$ is some interval of variable Np. Now we can define the Np-dependent effective γ and μ similarly to the way employed by Lam for the SAW on a diluted lattice [25],

$$\gamma_x \equiv 1 + \frac{I_H(x,x_0) - xQ_H(x) + x_0Q_H(x_0)}{H[\ln(x-H) - \ln(x_0-H)]}, \tag{36}$$

$$\ln\overline{\mu}_x \equiv \frac{I_H(x,x_0) - [Q(x) - Q(x_0)]\,q_H(x,x_0)}{H(x-x_0)}, \tag{37}$$

where

$$Q_H(x) \equiv \ln \sigma_H(x), \tag{38}$$

$$I_H(x, x_0) \equiv \int_{x_0}^{x} Q_H(x')\, dx', \tag{39}$$

$$q_H(x, x_0) \equiv \frac{x \ln x - (x-H)\ln(x-H) - x_0 \ln x_0 + (x_0 - H)\ln(x_0 - H)}{\ln x - \ln(x-H) - \ln x_0 + \ln(x_0 - H)}. \tag{40}$$

A crucial relation between the above definitions and the Monte Carlo data can be established by

$$\sigma_H(Np) = \lim_{A(1,p)\to\infty} \frac{A(N,p)}{A(N - H/p, p)}, \tag{41}$$

where $A(N,p)$ is the number of successful realizations of N-step PSAW's with *gauche* probability p and thus $A(1,p)$ equals the total number of starts at the origin. The role of interval $H = \Delta(Np)$ becomes clear when the simulation data are obtained for every $\Delta N = H/p$ steps. Simpson's rule is again used for the numerical integration Eq. (39) and the results for γ_{Np} and $\overline{\mu}_{Np}$ against the inverse of the logarithm of Np are presented in Figs. 6 and 7, respectively. As we noticed for the exponent ν, there is a similar indication that γ_{Np} asymptotically approaches the full SAW value ($\approx \frac{7}{6}$). However, $\overline{\mu}$ seems to strongly depend on p even in the asymptotic limit as is the case for any nonuniversal quantities.

We now take up the flight model by itself and calculate the survivability defined by

$$S_M \equiv \frac{C_{M,\mathrm{SAF}}}{C_{M,\mathrm{RF}}}, \tag{42}$$

where $C_{M,\mathrm{SAF}}, C_{M,\mathrm{RF}}$ are the *weighted* number of M-segment self-avoiding and random flights, respectively. Let us further define the local survivability and attrition rate as the following:

$$\sigma_M \equiv \frac{S_M}{S_{M-1}}, \tag{43}$$

$$\pi_M \equiv 1 - \sigma_M. \tag{44}$$

S_M and σ_M can be equivalently defined in the language of Monte Carlo simulation by $\overline{A}_M/\overline{A}_1$ and $\overline{A}_M/\overline{A}_{M-1}$ in the limit $\overline{A}_1 \to \infty$, respectively, where $\overline{A}_M$ is the number of realizations of M-segment self-avoiding flights.

It has been noted that the statistics of the PSAW model as a function of the number of steps is equivalent to that of this flight model as a function of its *contour* length. It should be further noted that the number of persistent segments in an N-step PRW is sharply peaked at Np for sufficiently large N and the contour length distribution of M-segment random flight is sharply peaked at its average, M/p, which is proved in Appendix A. Therefore the statistics of the flight model with the number of the segments $M = Np$ should become very close to that of the PRW (PSAW) with the number of steps N as $M = Np$ becomes large. This aspect is manifestly shown in Fig. 8, where the probability density functions for the PSAW (solid line) and the self-avoiding-flight model (dotted line) with $p = 0.1, 0.01$ and $M(= Np) = 5, 50$ are presented. These are obtained by Monte Carlo sampling of more than two million realizations. The complex structure of PSAW density functions for $Np = 5$ is not due to the statistical fluctuation but to its inherent property which does not seem to be widely recognized in the literature [26]. For $Np = 50$, however, there is little difference

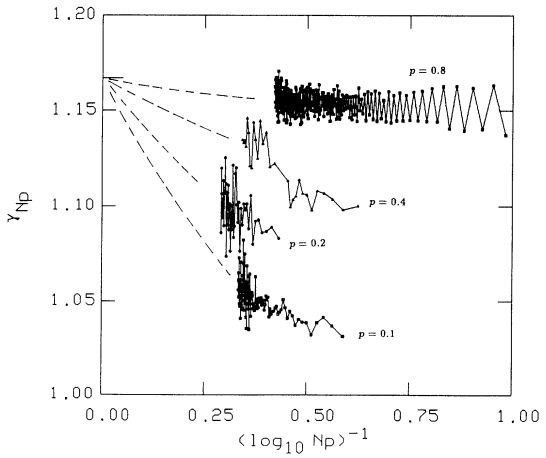

FIG. 6. The effective exponent γ_{Np} defined by Eq. (36) for the PSAW on the simple-cubic lattice. Dashed lines are drawn for a visual aid to show the asymptotic limit of γ_{Np} as $N \to \infty$ for any fixed p. In $d = 3$, $\gamma \approx 1.17$ for the ordinary SAW.

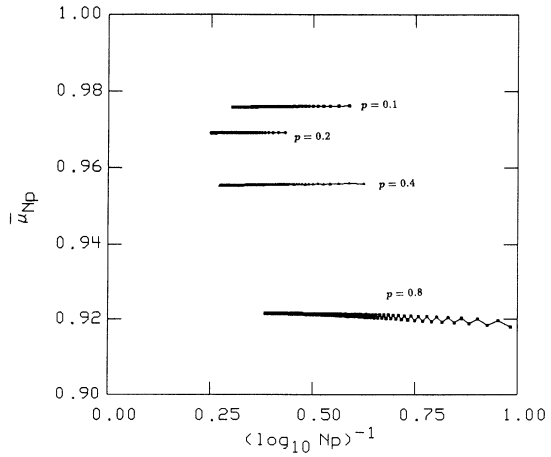

FIG. 7. The ratio of the effective coordination number of the PSAW to that of the PRW for the simple-cubic lattice defined by Eq. (37). It approaches unity as p becomes smaller without showing any universal asymptotic behavior.

between the two density functions. We will discuss this difference in more detail in Appendix A.

To calculate π_M [Eq. (44)], we consider the probability $\mathcal{P}_j^{(M)}$ that the first intersection for the M-segment flight is made by the Mth segment hitting the $(M-j+1)$th segment. (Intermediate *turning points* in the chain are taken to belong to only one segment as the *starting point.*) Then

$$\pi_M = \sum_{j=1}^{M} \mathcal{P}_j^{(M)}. \tag{45}$$

Obviously, on the sc and bcc lattices, $\pi_1 = \pi_2 = \pi_3 = 0$ because $\mathcal{P}_j^{(M)} = 0$ for $M = 1, 2, 3$. We will restrict the calculation to the sc lattice, obtain exact expressions for π_M up to $M = 6$, and then make an approximation as

$$\pi_M \approx \pi_6 \quad \text{for } M \geq 7 \quad \text{as } p \to 0. \tag{46}$$

Now let us compute $\mathcal{P}_j^{(M)}$ for $M = 4, 5, 6$, which are the first few nonzero terms in Eq. (45). Figure 9(a) shows the only possibility that the crossing occurs for $M = 4$. Note that the relative orientation of the first two segment (1 and 2 drawn in thick lines) is always the same and there are four possible directions in which each new segment can go. Thus

$$\begin{aligned}\mathcal{P}_4^{(4)} &= \frac{1}{4} \times \frac{1}{4} \times \text{Prob}(l_3 \leq l_1, l_4 \geq l_2) \\ &= \left(\frac{1}{4}\right)^2 \sum_{l_1,l_2=1}^{\infty} P(l_1)P(l_2) \sum_{l_3=1}^{l_1} P(l_3) \sum_{l_4=l_2}^{\infty} P(l_4) \\ &= \left(\frac{1}{4}\right)^2 \left(\frac{1}{2-p}\right)^2,\end{aligned}$$

where $P(l_i)$ is the segment size distribution [Eq. (24)]. Similarly, for five segment flights, Fig. 9(b), diagram i shows the only possible way for the fifth segment to hit the first segment. (Remember that the first turning point belongs to the second segment, not to the first.) Thus

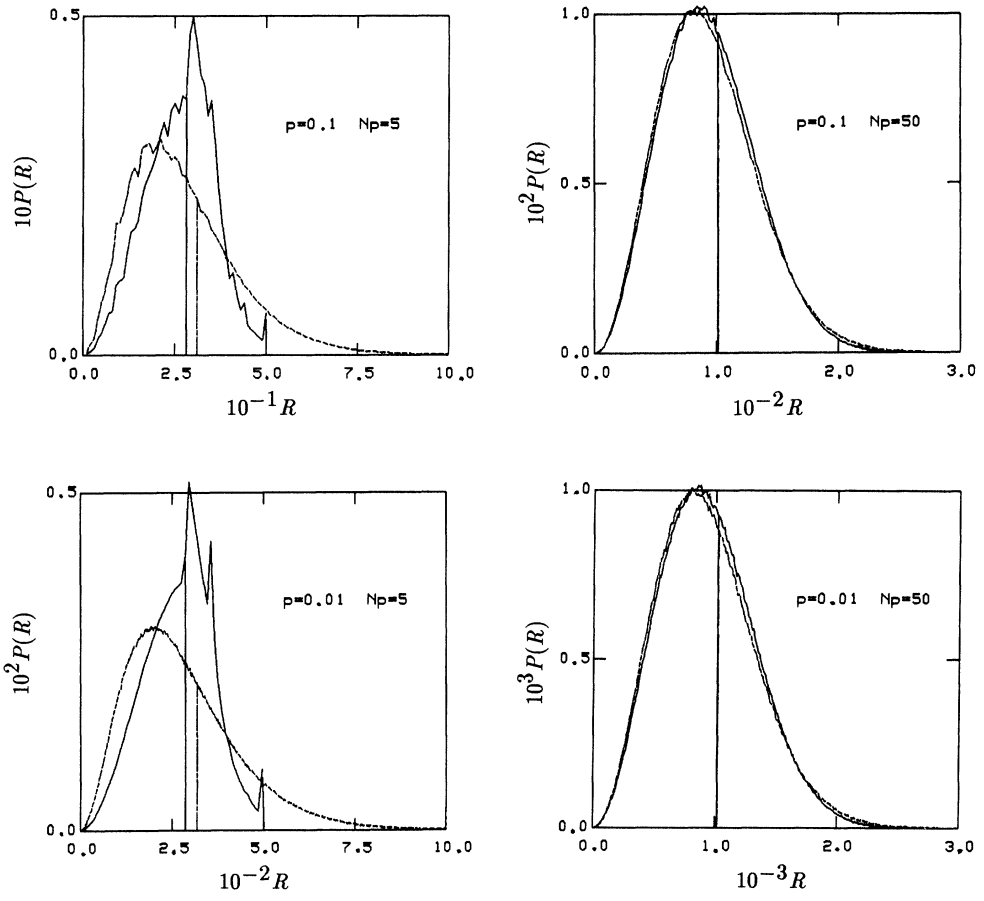

FIG. 8. Comparison of radial distributions of the end-to-end distances of the PSAW (solid line) and the flight model (dotted line) whose number of jumps (M) is such that its average contour length (M/p) is equal to the length of the PSAW (N). Vertical lines (solid and dotted) indicate the respective mean end-to-end distances. These are for the simple cubic lattice. For more details, see Appendix A.

$$\mathcal{P}_5^{(5)} = \left(\frac{1}{4}\right)^3 \text{Prob}(l_3 \geq l_1 + 1, l_4 = l_2, l_5 \geq l_3 - l_1) = \left(\frac{1}{4}\right)^3 \frac{p(1-p)}{(2-p)^3}.$$

It should be noted that $\mathcal{P}_4^{(5)} \neq \mathcal{P}_4^{(4)}$ since in such a case as Fig. 9(b), diagram ii the existence of the first segment (dashed line) matters in forming a four-segment loop in contrast to the case like Fig. 9(b), diagram iii. Thus

$$\mathcal{P}_4^{(5)} = \left(\frac{1}{4}\right)^3 \text{Prob}(l_4 \leq l_2 - 1, l_5 \geq l_3) + \frac{3}{4}\mathcal{P}_4^{(4)} = \left(\frac{1}{4}\right)^3 \frac{4-p}{(2-p)^2}.$$

This procedure becomes rapidly complicated as the number of segments increases: To calculate $\mathcal{P}_6^{(6)}$, for example, we need to compute probabilities for 15 diagrams like diagrams i and ii of Fig. 9(c), which are *distinct* as far as the relative direction and size relations of the segments are concerned. Here we simply present the final result of $\mathcal{P}_j^{(6)}$'s [again, $\mathcal{P}_5^{(6)} \neq \mathcal{P}_5^{(5)}$ and $\mathcal{P}_4^{(6)} \neq \mathcal{P}_4^{(4)}$ due to the presence of the first one or two segments; see diagrams iii and iv of Fig. 9(c)]:

$$\mathcal{P}_6^{(6)} = \left(\frac{1}{4}\right)^4 \left(\frac{(1-p)^2(16-15p+5p^2)}{(2-p)^4(3-3p+p^2)} + p\right),$$

$$\mathcal{P}_5^{(6)} = \left(\frac{1}{4}\right)^4 \frac{p(1-p)(10-11p+4p^2)}{(2-p)^3(3-3p+p^2)},$$

$$\mathcal{P}_4^{(6)} = \left(\frac{1}{4}\right)^4 \frac{1}{(2-p)^2}\left(15 + \frac{(1-p)^2(5-4p+p^2)}{(2-p)(3-3p+p^2)} - 3p\right).$$

One can easily observe some general features from these calculations for $\mathcal{P}_j^{(M)}$ which serve to justify the approximation (46) on the simple cubic lattice: First of all, if the segments are not all in the same plane [e.g., Fig. 9(c), diagram ii], the contribution of that diagram to the crossing probability $\mathcal{P}_M^{(M)}$ has the leading term proportional to p. This is because a combination of a group of segment sizes must be *exactly* the same as another combination for the last segment to hit the first segment. Moreover, this is also true for the case in which the intersection occurs with the first and last segments in the same coordinate direction for the same reason [e.g., Fig. 9(b), diagram i]. Therefore all constant terms in $\mathcal{P}_M^{(M)}$ come from diagrams of planar polygons with an even number of sides made by the intersection between the first and last segments. This implies that there is no constant term in $\mathcal{P}_M^{(M)}$ if M is an odd integer.

Another point is that the contribution of each diagram to the crossing probability consists of two factors, one from the choice of segment directions and the other from the segment size relations, the former giving rise to $(\frac{1}{4})^{M-2}$ for the sc lattice.

It should be that the above points also apply for $\mathcal{P}_j^{(M)}, j < M$ and that $\mathcal{P}_j^{(M)} \approx \mathcal{P}_j^{(j)}$ as $p \to 0$. Therefore, as far as the constant terms are concerned, each term in the summation of Eq. (45) is roughly an order of magnitude less than its previous term. Taking terms up to linear in p, we arrive at

$$\pi_4 \approx \frac{1}{64} + \frac{p}{64}, \quad \pi_5 \approx \frac{1}{64} + \frac{7}{512}p,$$
$$\pi_6 \approx \frac{103}{6144} + \frac{35}{2048}p,$$

and using Eqs. (43), (44), and (46),

$$S_M = \prod_{i=1}^{M} \sigma_i \approx S_5(1-\pi_6)^{M-5} \quad \text{for } M \geq 5, \tag{47}$$

where $S_5 = (1-\pi_4)(1-\pi_5)$. Substituting actual numbers into Eq. (47) for small p, we obtain the final form of approximation:

$$S_M \approx \left(\frac{63}{64}\right)^2 \left(\frac{6041}{6144}\right)^{M-5} e^{-\frac{105}{6041}p(M-5)} \quad \text{for } M \geq 5. \tag{48}$$

In fact, the right-hand side of the above equation should be an approximate upper bound of S_M since the attrition π_M is underestimated by Eq. (46). We present our Monte Carlo result for S_M with $p = 10^{-1}, 10^{-2}, 10^{-4}, 10^{-6}$ and

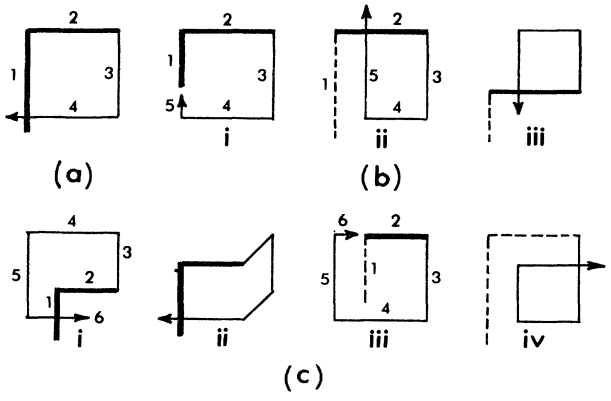

FIG. 9. Some examples (incomplete list) of distinct configurations of the flight model with 4, 5, and 6 segments on the simple cubic lattice which give nonzero contributions to $\mathcal{P}_j^{(M)}$ in Eq. (45). All segments in each diagram are on the same plane except for diagram ii in (c). Arabic numbers are labels for individual segments in the flight.

TABLE I. The global survivabilities of the flight model [S_M as in Eq. (42)] and PSAW [$S(Np)$ as in Eq. (34)] from our Monte Carlo data (simple cubic lattice). Numbers in parentheses are the predictions of an approximate analytic calculation for the flight model [Eqs. (47) and (48)] which serve as an approximate upper bound when p is small.

	$M = Np = 10$			$M = Np = 100$	
p	Flight model	PSAW	p	Flight model	PSAW
10^{-1}	0.872 (0.880)	0.854	10^{-1}	0.104 (0.164)	0.105
10^{-2}	0.886 (0.889)	0.872	10^{-2}	0.173 (0.191)	0.173
10^{-4}	0.888 (0.890)	0.873	10^{-4}	0.183 (0.194)	0.183
10^{-6}	0.888 (0.890)	0.874	10^{-6}	0.183 (0.194)	0.183

$M(= Np) = 10, 100$ in Table I.The prediction [Eq. (48)] is very accurate for the flight model for smaller M and reasonably good for the PSAW model for small p and Np. The attrition of the PSAW in the Gaussian regime has been numerically analyzed by Lee and Nakanishi [12]. Their result was that the survival probability of the PSAW in the Gaussian regime is proportional to $e^{-\lambda Np}$ with $\lambda \approx 0.0186$ for the sc lattice. We note that the right-hand side of Eq. (48) can be expressed as $\sim e^{-\lambda_1 Np - \lambda_2 Np^2}$ with M replaced by Np and their λ corresponds to $\lambda_1 \equiv \ln(6144/6041) \approx 0.0169$.

Finally, we point out that for the approximations (46) and (48) to be valid, M should be small enough such that $Mp \ll 1$. If M itself is much larger than unity but $p \to 0$, then this should correspond to the Gaussian regime of the PSAW with $Np^2 \ll 1$. Therefore, to go beyond the Gaussian regime, N should be greater than p^{-2} at least, which sets the lower limit of exponent y to be 2.

IV. ANALYSIS OF PREVIOUS EXPERIMENT

Some years ago, Murakami, Norisuye, Fujita [19] reported the result of light scattering and other measurements performed on an extremely stiff linear polymer, poly-hexyl-isocyanate (PHIC) with narrow molecular weight dispersion in hexane solvent at room temperature. In particular, they reported the z-averaged radius of gyration and analyzed its molecular weight dependence in terms of the Benoit-Doty theory [2] for the Kratky-Porod wormlike chain [1].

Although they recognized the onset of the excluded-volume effect at large molecular weight, no quantitative analysis of this aspect was given, presumably because there were no theoretical results to compare their data with. It is the aim of this section to attempt some quantitative analyses on their result in the context of the discussions presented in previous sections.

We first convert the original data for the radius of gyration given in terms of the experimental parameters (see Table I and Fig. 7 in Ref. [19]) into those in terms of the dimensionless, stiff chain parameters (N, p) with the lengths being in units of the monomer size (a) in the direction tangent to the contour. That is, from the result that the molar mass per unit contour length $M_L = 715 \pm 15$ nm^{-1}, the persistent length $q = 42 \pm 1$ nm, and the molar mass of the monomer $M_0 = 127$, we calculate the monomer length $a = M_0/M_L = 0.178 \pm 0.003$ nm and the *gauche* probability $p = a/q = 0.0042$. The diameter of the cylinder D, however, seems to assume two different values, namely, 1.6 and 2.5 nm, depending on what measurement it is estimated from. We will use these two values as the range of estimate for D and obtain the monomer anisotropy of $b = D/a = 9.0$–14. Hence the block level *gauche* probability $p' \equiv bp = 0.038$–0.059. Although the monomer anisotropy is not exactly disklike (the structure of poly-alkyl-isocyanates being in general helical), we treat monomers as effectively disks in this discussion.

In Fig. 10, those converted data for the radius of gyration of PHIC (circles) with an appropriate overall factor are plotted against Np together with two other sets of PSAW simulation data [one for $p = 0.05$ (dots) and the other for $p = 0.77$ (crosses)] on the simple cubic lattice.

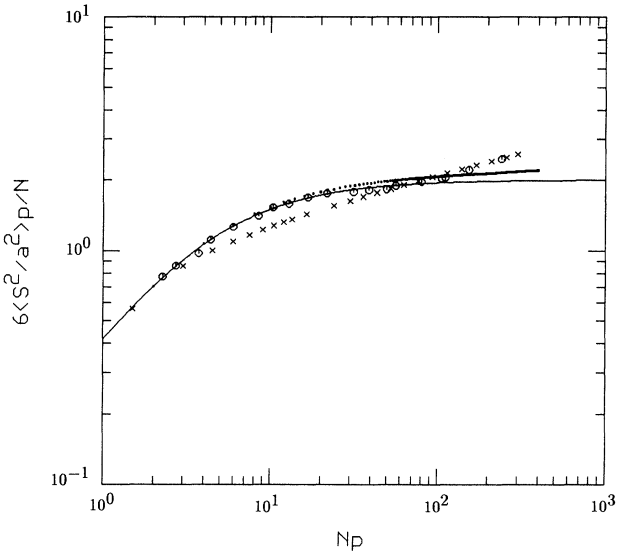

FIG. 10. The result of Murakami, Norisuye, and Fujita [19] (circles) on the radius of gyration (S) of poly-hexyle-isocyanate polymers is plotted in terms of PSAW parameters together with PSAW results on the simple cubic lattice with $p = 0.05$ (dots) and $p = 0.77$ (crosses). Solid line is the PRW result [Eq. (49)]. a in the ordinate label is the monomer size (contour length per monomer).

The solid line is the Gaussian fit for the radius of gyration:

$$\langle S^2 \rangle = \frac{N}{p}\left(\frac{1}{3} - \frac{1}{Np} + \frac{2}{(Np)^3}(e^{-Np} + Np - 1)\right). \tag{49}$$

Note that both the ordinate and the abscissa in Fig. 10 are invariant under the rescaling (18) for a fixed value of $\langle S^2 \rangle$. Therefore, even though the PHIC data points are plotted from original parameters, they would make the same plot with the isotropic block level parameters. To directly compare the experimental data of stiff chains with monomer anisotropy with the PSAW model, an appropriate rescaling like (18) is needed to eliminate the involvement of monomer anisotropy which is absent in the PSAW model. We will view the PHIC chain as a train of this isotropic blocks which are still stiff at the block level whenever they are compared with the PSAW model.

The crossover behavior of the experimental data from the Gaussian–to–excluded-volume regime can be compared with the predictions of the PSAW model in the the following ways.

First of all, the Gaussian regime itself seems to be rather close to the true Gaussian result (PRW) without the excluded-volume effect. As noted in previous sections, the end-to-end distance of the PSAW in the Gaussian regime is definitely larger than that of the PRW. This is the case for the radius of gyration as shown in Fig. 10 by the PSAW simulation result for $p = 0.05$. This value of p is chosen simply because it is about the mean of estimated block level *gauche* probabilities.

Secondly, we note that the behavior of the radius of gyration of PHIC starts to deviate from the Gaussian regime at around $Np \approx 80$ manifestly showing the onset of the excluded-volume effect thus allowing us to estimate from Eqs. (15) and (16)

$$y = 1 - \frac{\ln N^* p}{\ln bp} + \frac{\ln B}{\ln bp}, \tag{50}$$

where B is the proportionality constant in Eq. (15). The range of estimation for y is dependent on those of b (9.0–14) and B with $N^*p = 80$, $p = 0.0042$: If $B = 1$ is used, Eq. (50) will give $y = 2.3$–2.5. If B differs from unity by a factor of 2 (smaller or larger), then $y = 2.1$–2.8. As shown in the preceding section, the lattice results for this exponent determined by the behavior of the scaling function are essentially covered by this experimental estimation which is done from the finding of N^*. However, experimentally this crossover occurs abruptly, which is in great contrast to the PSAW, and yet the experiment gives the value for exponent y fairly close to that of the PSAW which was purely numerically estimated.

Lastly but not least, the slope in the log-log plot of the data points in the excluded-volume regime indicates that the Flory exponent suddenly takes on a value very close to the full SAW value of $\nu(\approx 0.59)$ immediately after the onset of the crossover. This suggests a possibility that the conformation of a real stiff chain undergoes some type of a phase transition as soon as the excluded-volume effect is felt.

One possibility of the chain conformation upon the crossover may be that a train of mutually repulsive blobs acts like a SAW, inside of which, however, it is rather like that of the PRW (because of the first point noted above). Since the crossover appears very sharp (the third point above), the geometrical boundary of a blob should be distinct with little overlap with other blobs. This might be realized by some sort of repulsive molecular field. It should be noted that this particular blob conformation is slightly different from the blob picture suggested in Sec. II in that the latter merely comes about from an arbitrary interpretation of the variable of the scaling function and if the blobs did exist in the PSAW, they must be overlapping significantly, with the Gaussian regime of the PSAW, not with the PRW, inside each blob. Also, the experimental points with the SAW exponent correspond to regions of a few blobs, whereas a SAW of only a few steps does not show the asymptotic exponent.

Another possibility related to the sudden change of the Flory exponent may be that, having nothing to do with the blob picture, the chain breaks up into nearly isotropic units (essentially our "blocks") which are no longer stiffly joined, i.e., a sudden shattering occurs. Thus, lost persistence is more than compensated for by the excluded-volume interaction of this new self-avoiding walk of the blocks. In Fig. 10, the part of the PHIC data points which falls in the excluded-volume regime seem to be as if they were a part of PSAW data with $p = p'' \equiv 0.77$ (for the ordinary SAW, $p = 0.8$.). This may suggest that at $N = N^*$ beyond the newly formed isotropic blocks perform a PSAW with $p = p''$.

If any of these possibilities were true for a real polymer, there may be some kind of phase transition as the molecular weight increases. We are unaware of any other experimental work that probes the conformation of the real stiff polymer in more detail for the excluded-volume effect. A more quantitative theoretical study would require a new model incorporating an appropriate phase transition at the onset of the excluded-volume effect.

V. SUMMARY AND DISCUSSION

The persistent self-avoiding walk model has been used to study the conformation of a stiff linear polymer in a good solvent. The general behavior of the size R of such very stiff chains in three dimensions as a function of the degree of polymerization N is characterized by three regimes, namely, rodlike ($R \sim N$), Gaussian ($R \sim N^{\frac{1}{2}}$), and excluded-volume ($R \sim N^{\nu_F}, \nu_F \approx 0.59$). Two crossovers between these regimes, termed rod-to-flexible and Gaussian–to–excluded-volume, can be expressed by some scaling functions in terms of scaling variables Np and $Np^y (y > 1)$, respectively, where N and p^{-1} tend to infinity while an appropriate scaling variable is being kept finite. (p is the *gauche* step probability, the usual SAW

corresponding to $p = 0.8$ on the simple cubic lattice.)

The crossovers are expected to occur when the chain length becomes such that the corresponding scaling variables are of the order of unity ($N^+p \approx 1, N^*p^y \approx 1$). A Flory argument predicts $N^* \sim p^{-3}b^{-2}$, where b is the ratio of the diameter to the thickness of the monomer, which implies that $y = 3$ but the monomer anisotropy causes the excluded-volume effect to set in for shorter chains. Beyond the Flory theory, a scaling argument leads us to an expression for the excluded-volume regime $R \sim N^{2\nu}p^{-\alpha}b^{-\beta}$ for $N \gg N^* \sim p^{-y}b^{-z}$, where $z = y-1$, $\alpha = 1-(2\nu-1)y$, $\beta = (y-1)(2\nu-1)$. A view of very long stiff chains as a train of mutually repelling blobs inside which the chain is in the Gaussian regime reproduces the results of scaling and Flory arguments if Np^y is interpreted as the number of blobs forming the chain.

An extensive Monte Carlo simulation of the PSAW shows that even though the Gaussian–to–excluded-volume crossover occurs extremely slowly for stiff chains, there exists a clear indication that the effective exponents like ν_N and γ_N approach the full SAW values asymptotically. Results on different types of lattices appear to support the strong universality for the second crossover scaling function up to a metric factor. Numerical estimation for exponent y obtained from the best data collapsing for the scaling variable Np^y suggests different values of $y \approx 2.5$ or 2.9 depending on the choice of the scaling function. The estimation of y from experimental data of a real polymer (poly-hexyl-isocyanate) is done by directly setting $N^*p^y = 1$, which gives rise to $y \approx 2.3$–2.5 or 2.1–2.8 as the proportionality constant in $N^* \sim p^{-y}b^{-(y-1)}$ is chosen to be 1–$2^{\pm 1}$. But in the real polymer case, the excluded-volume regime ($\nu \approx 0.59$) immediately follows rather sharply defined N^* in great contrast to the PSAW result, which seems to indicate a certain type of structural phase transition.

A flight model on a discrete lattice which has the segment size distribution identical to the persistence length distribution of the PRW (PSAW) and makes a turn at each jump is shown to have asymptotically the same statistics as that of the PRW (PSAW) in the many-segment limit if the latter is expressed in terms of the mean number of persisent segments Np. An approximate analytic expression of survival probability of this self-avoiding-flight model is obtained for the $p \to 0$ limit and is shown to be a good approximation for that of the PSAW in the Gaussian regime. Moreover, this approximation allows us to determine the lower limit of exponent y to be 2. We also note that the spatial distribution of the end-to-end distance of the PSAW having not too many segments is very complex showing multiple sharp peaks. This feature could be explained in terms of the competition between the entropy and stiffness effects. (See Appendix A.)

Finally, we believe that more analytic methods like renormalization-group calculations may be necessary to determine exponent y and new models that can incorporate, for instance, the energetics between side groups of the stiff chain can be instrumental to understand the sudden crossover which seems to exist in real polymers.

ACKNOWLEDGMENTS

We would like to thank Woods Halley, David Atkatz, and Amos Maritan for discussions. This work was supported in part by a grant from the Office of Naval Research.

APPENDIX A: PROBABILITY DISTRIBUTIONS OF WALK AND FLIGHT MODELS

The probability that an N-step PRW has t turns (or *gauche* steps) is

$$P_N(t) = \binom{N-1}{t} p^t q^{N-1-t}, \quad t = 0, \ldots, N-1 \qquad \text{(A1)}$$

where p is the *gauche* probability and $q \equiv 1-p$. Expanding $\ln P_N(t)$ in Taylor series around its maximum at $t = \bar{t}$, we get, with $\bar{t} \approx Np$ and $\Delta \approx \sqrt{Npq}$,

$$P_N(t) \approx \frac{1}{\sqrt{2\pi}\,\Delta} e^{-\frac{1}{2}[(t-\bar{t})/\Delta]^2}, \qquad \text{(A2)}$$

if $Npq \ll 1$. This implies that the distribution for the number of turns (hence the segments) in the PRW is sharply peaked at $t = Np$ (the average number of persistent segments) with relative width $\Delta/\bar{t} \sim 1/\sqrt{Np} \ll 1$ in the many-segments limit.

On the other hand, the probability that the contour length of an M-segment flight (on a discrete lattice) is n is

$$\overline{P}_M(n) = \sum_{l_1=1}^{\infty} \cdots \sum_{l_M=1}^{\infty} \prod_{i=1}^{M} P(l_i)\, \delta_{n,\mathbf{L}_M}, \qquad \text{(A3)}$$

where $\mathbf{L}_M = \sum_{i=1}^{M} l_i$ and $P(l_i)$ is defined in Eq. (24). Considering the number of possible ways in which $M-1$ turns can occur along the contour of length n, Eq. (A3) can be written as

$$\overline{P}_M(n) = \binom{n-1}{M-1} p^M q^{n-M}, \quad n = M, \ldots, \infty. \qquad \text{(A4)}$$

We again expand $\ln \overline{P}_M(n)$ around its maximum at $n = \overline{n}$ arriving at, for $qM \gg 1$,

$$\overline{P}_M(n) \approx \frac{1}{\sqrt{2\pi}\,\Delta'} e^{-\frac{1}{2}[(n-\overline{n})/\Delta']^2}, \qquad \text{(A5)}$$

where $\overline{n} = M/p = \langle n \rangle$ and $\Delta' = \sqrt{qM}/p$ thus the relative width $\Delta'/\overline{n} \sim 1/\sqrt{M} \ll 1$. Equations (A2) and (A5) establish the statistical equivalence between the PRW and the suggested flight model in the many-segment limit with $M = Np$ and we believe that the same is true for the case in which the excluded-volume effect is present.

We now express the spatial probability distributions of the PRW, $W_N(\mathbf{r})$, and the flight model, $\overline{W}_M(\mathbf{r})$, in more quantitative terms. For the PRW, each *gauche* step is weighted by $p/(z-2)$ (z is the coordination number of the lattice) and the first step by $1/z$ for a particular path of end-to-end displacement $\mathbf{r}$. Thus

$$W_N(\mathbf{r}) = \frac{1}{z}\sum_{t=0}^{N-1} g_N(t,\mathbf{r})\left(\frac{p}{z-2}\right)^t q^{N-1-t}, \qquad \text{(A6)}$$

where $g_N(t,\mathbf{r})$ is the number of N-step walks with t *gauche* steps whose end-to-end displacement is $\mathbf{r}$, and

$$\sum_{\mathbf{r}} g_N(t,\mathbf{r}) = z\binom{N-1}{t}(z-2)^t.$$

For the flight model, one can first write down

$$\overline{W}_M(\mathbf{r}) = \sum_{\mathbf{l}_1}\cdots\sum_{\mathbf{l}_M}\prod_{i=1}^{M} P(\mathbf{l}_i)\,\delta_{\mathbf{r},\mathbf{L}_M}. \qquad \text{(A7)}$$

where $\mathbf{L}_M = \sum_{i=1}^{M}\mathbf{l}_i$. Note that the distribution for a *vector* segment $P(\mathbf{l}_i)$ is simply that for the segment size [Eq. (24)] divided by the number of possible directions in which the segment can make a turn, namely, z for the first segment and $z-2$ for all others. Thus we obtain

$$\overline{W}_M(\mathbf{r}) = \frac{z-2}{z}\left(\frac{p}{(z-2)q}\right)^M \sum_{n=M}^{\infty}\overline{g}_M(n,\mathbf{r})\,q^n, \qquad \text{(A8)}$$

where $\overline{g}_M(n,\mathbf{r})$ is the number of M-segment flights with contour length n whose end-to-end displacement is $\mathbf{r}$, and thus

$$\overline{g}_M(n,\mathbf{r}) = g_n(M-1,\mathbf{r}).$$

Note that the $\mathbf{r}$ in W_N has the upper cutoff $|\mathbf{r}| = N$, whereas there is none in $\overline{W}_M$.

To get the radial distributions from Eqs. (A6) and (A7) as in Fig. 8, a suitable summation needs to be performed:

$$w^r(R) = \frac{1}{\Delta R}\sum_{R\le|\mathbf{r}|<R+\Delta R} w(\mathbf{r}), \qquad \text{(A9)}$$

where w is to be replaced by either W_N or $\overline{W}_M$ as appropriate. Equation (A9) reduces to a series of Δ functions in the limit $\Delta R \to 0$ because of the discreteness of the lattice. But even for a finite ΔR, Eq. (A9) for the PRW and PSAW (Figs. 8 and 11) has a peculiar structure with major peaks and minor oscillations which is absent in the flight model when the (average) number of segments is not very large. Why? It is very difficult to answer by an approximation for Eqs. (A6) or (A7) since in this case Np is not large enough for any kind of useful approximation even if N itself may be large.

However, one may get some insight for understanding this feature by looking at the $|\mathbf{r}| = N$ (fully stretched chain) case [26] for Eqs. (A6) and (A9), in particular. The contribution to W_N in Eq. (A6) comes only from the $t = 0$ term so that $W_N^r(N) = (1-p)^{N-1}$. Now consider a case in which $|\mathbf{r}|$ is only slightly less than N in Eq. (A6) such that not too many turns are allowed. Then the $t = 0$ term in W_N is absent because there must be at least one turn to achieve the desired configuration and thus $W_N^r(R)$ contains only terms in some positive powers of p. Moreover, since the entropy factor g_N in Eq. (A6) does not very rapidly change in the region $|\mathbf{r}| \approx N$, the stiffness factor (terms proportional to p or its higher orders) would readily render W_N^r very small if p is small enough. On the other hand, $W_N^r(N) \approx \text{const}\ (e^{Np})$ for small p with fixed Np, which implies that this feature becomes more prominent for smaller p. Explanations for other peaks may be made in terms of a similar competing effect between the entropy and stiffness factors for a given set of t and R for fixed N, even if it is not easy to pin down where they occur from any simple argument.

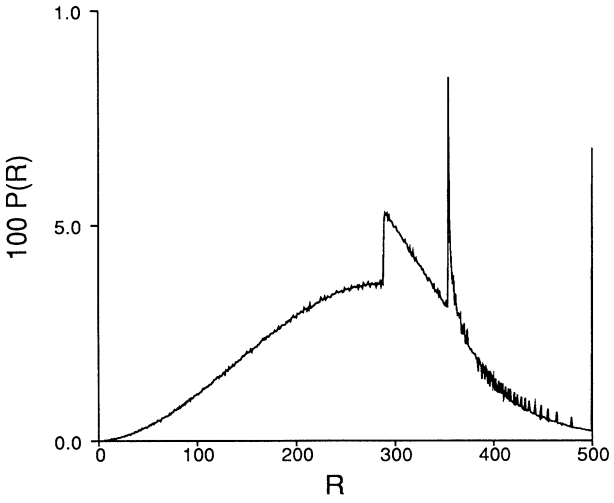

FIG. 11. Radial probability distribution of the PRW with $p = 0.01$, $N = 500$, and $\Delta R = 1$ in Eq. (A9). The local peaks become sharper for smaller ΔR. PSAW (not shown) has almost identical distribution for this set of parameters.

For the flight model, however, $R = M/p$ is not special in the sense it is for the PRW (the upper cutoff of the chain size) since the segment size of the flight is unlimited only having a probability distribution. Moreover, the stiffness factor p^M is out of the summation in Eq. (A7), that is, it is constant for all $\mathbf{r}$ not being coupled with the entropy factors $\overline{g}_M$ which by themselves constitute an infinite summation. Even though there still exist more favorable sets of M and R for the entropy factor with given n, that effect gets smeared out by the summation over n. Therefore $\overline{W}_M^r(R)$ is determined only by the entropy factors and the summation in Eq. (A9), which turns out to be a smooth function of R even for a relatively small M (5 in this case).

APPENDIX B: MONTE CARLO METHOD

In this appendix, we discuss the loop-checking methods for self-avoiding walks and flights on a discrete lattice in more detail and present important simulation parameters and computing times.

The idea of the hash-coding method for loop-checking when a walk is realized by *steps* hinges on the fact that every site on a discrete lattice can be assigned a unique label by a simple FORTRAN code like $\text{mod}(\mathbf{q}\cdot\mathbf{r}, K) + K$, where $\mathbf{q}$ is a constant vector, $\mathbf{r} = (x,y,z)$ is the dis-

TABLE II. Parameters used and number of the longest walks obtained in our Monte Carlo simulations of the PSAW model on the simple cubic (otherwise specified) lattice. Data for $p \leq 0.1$ were obtained mainly from the equivalent flight model as explained in Sec. III. The number of stages, length of stages, and the number of trials per stage refer to the parameters of a standard enrichment technique.

p	Number of stage	Length of stage (in units of Np)	Number of trials per stage	Number of walks First step	Last step
0.8	20	20	5	8 794 990	3 000 000
0.4	120	39.6	6	1 470 036	100 238
0.2	193	51.6	5	1 325 860	108 071
0.1	20	100	11,10,9	3 086 425	130 578
0.1 (bcc)	10	100	4	1 603 228	100 011
0.1 (fcc)	20	50	4	124 448	30 009
0.1 (Diamond)	2	500	5	1 530 155	10 000
0.05	40	100	8	1 095 364	121 965
0.02	58	104	7	1 533 716	102 222
0.01	101	99	6	2 628 996	80 364
0.01 (bcc)	1	100	1	218 953	100 000
0.01 (fcc)	1	100	1	756 828	100 000
0.01 (Diamond)	1	100	1	124 851	100 000
10^{-4}	10	100	6	680 706	200 004
10^{-6}	10	100	5	3 510 845	200 011

placement of a site, and K is some positive integer. This will partition the whole lattice points into $2K+1$ categories so that the loop-checking can be done only among a small number of sites in the same category. Thus an array (*hash*) of size $2K+1$ is needed to store the newest step numbers which fell into each category and another array (*chain*) of size equal to the maximum number of steps to keep track of the most recent previous step in the same category of all steps generated.

This simple method cannot be directly used to detect an intersection between two *segments*. So we introduce *supercategories* represented by separate arrays and restrict our discussion only to the simple cubic lattice. Each segment belongs to three supercategories: For example, a segment generated in the x direction belongs to supercategories $[xx]$, $[xy]$, and $[xz]$. This segment is further categorized by $\mathrm{mod}(q_1 y + q_2 z, K_1) + K_1$ in $[xx]$, by $\mathrm{mod}(q_3 z, K_2) + K_2$ in $[xy]$, and by $\mathrm{mod}(q_3 y, K_2) + K_2$ in $[xz]$. Thus $[xx]$ contains segments only in the x direction, $[xy]$ contains those in either the x or y direction, and $[xz]$ contains those in either the x or z direction. For each supercategory, *hash* and *chain* arrays as described in the preceding paragraph are needed for bookkeeping and the loop-checking is made only among segments belonging to the same categories using the algorithm in Ref. [24].

The PSAW realization using the flight algorithm becomes particularly advantageous as p becomes smaller. It wins over the walk algorithm by nearly a factor of 2 for $p = 0.1$ and by more than a factor of 100 for $p = 0.01$ as far as the computing speed is concerned. Our data for $p \leq 0.1$ were obtained mainly from the flight algorithm.

We also used the well-known enrichment technique [23] to compromise the computing time with the attrition inherent in growing self-avoiding walks and flights. Special care must be taken when the enrichment is done for the flight model to get the PSAW statistics (by keeping track of the contour length). The correct method is that the enrichment should be done at segments which first reach the perdetermined contour lengths. If, instead, the flights were enriched at a predetermined number of segments, then in effect the enrichment would be done always at *gauche* steps when viewed in the frame of the PSAW, which entails unduly more weights on *gauche* steps. This generally produces a minor oscillation in the end-to-end distance of the PSAW the period of which is related to the length of the enrichment stage. This oscillation dies out as the chain becomes longer only reducing the the end-to-end distance by a small factor. Our $p = 0.01$ data for the end-to-end distance up to $Np = 10^4$ were obtained using the latter method but the correction for $Np > 10^3$ turned out to be less than 1% which is even less than their standard deviations. Enrichment parameters and number of PSAW realizations for various values of p are presented in Table II.

Computers that were used in this work and their CPU times are as follows: 60 h on ISI 68020 V24, 296 h on Sequent Symmetry S-81, 312 h on DEC VAX 8800, 256 h on ETA-10 and Cray 2, 15 h on CDC Cyber 205, 1100 h on Stardent P-3000 Mini-Supercomputer, and 708 h on Silicon Graphics 4D/340 Mini-Supercomputer.

[1] O. Kratky and G. Porod, Rec. Trav. Chim. Pays-Bas **68**, 1106 (1949).
[2] H. Benoit and P. Doty, J. Phys. Chem. **57**, 958 (1953).
[3] D. W. Schaefer, J. F. Joanny, and P. Pincus, Macromolecules **13**, 1280 (1980).
[4] S. M. Bhattacharjee and M. Muthukumar, J. Chem. Phys. **86**, 411 (1987).
[5] Robert Cook, Macromolecules **20**, 1961 (1987).

[6] V. Privman and N. M. Švrakić, J. Stat. Phys. **50**, 81 (1988).
[7] P. J. Flory, *Principles of Polymer Chemistry* (Cornell University, Ithaca, NY, 1953).
[8] P. J. Flory, *Statistical Mechanics of Chain Molecules* (Interscience, New York, 1969).
[9] P. G. de Gennes, *Scaling Concepts in Polymer Physics* (Cornell University, Ithaca, NY, 1979).
[10] W. K. Schroll, A. B. Walker, and M. F. Thorpe, J. Chem. Phys. **76**, 6384 (1982).
[11] J. J. G. Molina and J. G. de la Torre, J. Chem. Phys. **87**, 4026 (1986).
[12] S. B. Lee and H. Nakanishi, Phys. Rev. B **33**, 1953 (1986).
[13] S. B. Lee and H. Nakanishi, J. Phys. A **20**, L457 (1987).
[14] J. W. Halley, D. Atkatz, and H. Nakanishi, J. Phys. A **23**, 3297 (1990).
[15] J. W. Halley, H. Nakanishi, and R. Sundararajan, Phys. Rev. B **31**, 293 (1985).
[16] V. Privman and S. Redner, Z. Phys. B **67**, 129 (1987).
[17] H. Nakanishi, J. Phys. (Paris) **48**, 979 (1987).
[18] M. L. Glasser, V. Privman, and A. M. Szpilka, J. Phys. A **19**, L1185 (1986).
[19] H. Murakami, T. Norisuye, and H. Fujita, Macromolecules **13**, 345 (1980).
[20] See, for example, L. P. Kadanoff, in *Proceedings of 1970 Varenna Summer School on Critical Phenomena*, edited by M. S. Green (Academic, New York, 1971); S.-k. Ma, *Modern Theory of Critical Phenomena* (Benjamin, Reading, MA, 1976).
[21] V. Privman and H. L. Frisch, J. Chem. Phys. **88**, 469 (1987).
[22] T. Odijk and A. C. Houwaart, J. Polym. Sci. Polym. Phys. Ed. **16**, 627 (1978).
[23] F. T. Wall, S. Windwer, and P. J. Gans, Methods Comput. Phys. **1**, 217 (1963).
[24] J. Moon and H. Nakanishi, Phys. Rev. A **40**, 1063 (1989).
[25] P. M. Lam, J. Phys. A **23**, L831 (1990).
[26] For the off-lattice case such as the randomly broken chain model, see Ref. [11] for a brief discussion of a similar point.